

POWER SPECTRUM SENSITIVITY AND THE DESIGN OF EPOCH OF REIONIZATION OBSERVATORIES

MIGUEL F. MORALES

Center for Space Research, Massachusetts Institute of Technology, 77 Massachusetts Avenue, Cambridge, MA 02139;
mmorales@space.mit.edu

Received 2004 June 29; accepted 2004 October 7

ABSTRACT

Recent theoretical developments for observing the epoch of reionization (EOR) have concentrated on the power spectrum signature of redshifted 21 cm emission. These studies have demonstrated the great potential of statistical EOR observations; however, the sensitivity calculations for proposed low-frequency radio arrays have been highly approximate. The formalism developed for interferometric measurements of the cosmic microwave background can be extended to three dimensions to naturally incorporate the line-of-sight information inherent in the EOR signal. In this paper we demonstrate how to accurately calculate the EOR power spectrum sensitivity of an array and develop scaling relationships that can be used to guide the design of EOR observatories. The implications for antenna distribution, antenna size, and correlator requirements on the EOR sensitivity are detailed.

Subject headings: cosmology: observations — radio lines: general

1. INTRODUCTION

In the last year significant advances have been made in understanding the characteristics of the redshifted 21 cm emission from the epoch of reionization (EOR) and how this signal can be separated from the contaminating foreground emission. It was originally believed that contamination from a host of strong foreground sources would overwhelm the EOR signal (Di Matteo et al. 2002), making observations all but impossible. In the fall of 2003 it was shown by Zaldarriaga et al. (2004) and Morales & Hewitt (2004) that differences in the frequency characteristics between the foreground contamination and the EOR emission could be used to identify the cosmological signal. In addition, these papers show how statistical techniques developed for measurements of the cosmic microwave background (CMB) could be extended to EOR observations. Recent theoretical advances by Furlanetto et al. (2004a, 2004b) have demonstrated that these statistical EOR observations can easily differentiate between various reionization histories.

The combination of new analysis methods, accurate theoretical calculations, and advances in low-frequency radio instrumentation have spawned several experimental EOR efforts. One remaining stumbling block for instrumental designers is the difficulty in predicting the sensitivity of a radio array to the EOR power spectrum. In § 2 we generalize the sensitivity calculations to accurately include both frequency information and the effects of antenna distribution. Then §§ 3 and 4 explore the effects of design choices on the EOR sensitivity and the implications for EOR arrays.

It is important to note that residual errors from subtracting foreground sources will contaminate the power spectrum. The sensitivity calculation presented here only includes the effects of the thermal noise and thus represents an upper limit on the signal-to-noise ratio that can be obtained by a given array. However, determining the noise-dominated sensitivity is still important for designing EOR observatories.

2. SENSITIVITY DERIVATION

As discussed in Morales & Hewitt (2004), the EOR produces a spherically symmetric three-dimensional power spectrum sig-

nal. This introduces a notational difficulty, since most of the theoretical work for the CMB uses spherical harmonics. Because the CMB signal forms a spherical two-dimensional surface on the sky, spherical harmonics are the natural orthogonal set. The m -terms of the spherical harmonics can be summed over, because the isotropy of space removes the rotational dependence, leaving the standard multipole l expansion of the CMB.

The EOR signal, however, is inherently three-dimensional and requires that an additional axis be added to the CMB analysis. Zaldarriaga et al. (2004) and Bharadwaj & Ali (2004) used spherical harmonic or two-dimensional Fourier transforms for each “step” in the line-of-sight distance (observed frequency) to produce a series of shells or planes that show the spatial structure in the sky dimensions and the real space positions in the line-of-sight distance. In these representations the signal in neighboring frequency slices is highly correlated because of the large amount of low-frequency power in the matter-density power spectrum.

Alternatively, a basis set can be chosen that extracts the spatial structure of the signal in all three dimensions and minimizes the correlation of the parameters. While there are several basis sets that could be used, we follow the approach of Morales & Hewitt (2004) and use the three-dimensional Fourier transform representation. If spherical sky effects can be ignored, the true signal is uncorrelated in this representation with the only correlation being introduced by the field of view and bandwidth of the observations. While all three approaches are effectively identical, calculating the sensitivity of an array is simpler using the three-dimensional expansion because of the independence of the measurements. The relationships between the image cube, the measured visibility cube used by Zaldarriaga et al. (2004) and Bharadwaj & Ali (2004), and the three-dimensional Fourier representation used here are depicted in Figure 1.

Section 2.1 briefly reviews the derivation of the EOR signal power spectrum in the three-dimensional Fourier representation, and § 2.2 derives the characteristics of the thermal noise and explains how to precisely calculate the power spectrum sensitivity. These relationships are then approximated in §§ 3 and 4 to explore the effects of array design on the sensitivity.

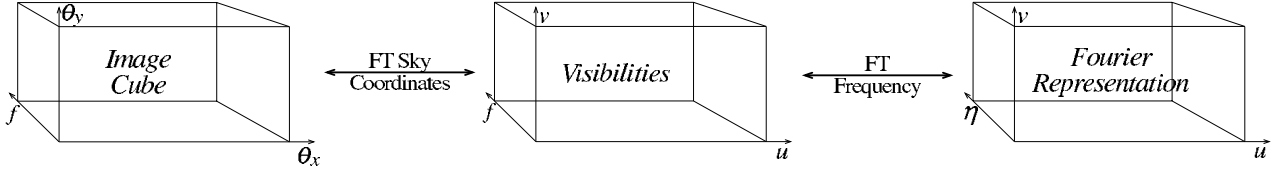


FIG. 1.—This diagram shows the Fourier transform relationships between the image cube, the measured visibilities, and the Fourier representation. For an interferometer, the fundamental observable is the visibility-frequency cube, which can then be transformed into either an image cube to show source locations (including line of sight) or the Fourier representation to analyze the spatial structure of the signal.

2.1. Signal Properties

The true distribution of the specific intensity of the EOR signal is given by

$$\Delta I_T(\mathbf{u}) = F_{H_I}(\mathbf{u}) \equiv C(\mathbf{u}) \frac{\rho_{H_I}(\mathbf{u})}{\langle \rho_H \rangle}, \quad (1)$$

where F_{H_I} gives the fluctuation in the neutral hydrogen emission. The vector \mathbf{u} describes the position in the three-dimensional Fourier space and is defined by $\mathbf{u} \equiv u\hat{i} + v\hat{j} + \eta\hat{k}$. The variables u , v , and η , in turn, are the wave numbers associated with the spatial positions on the sky θ_x , θ_y , and the frequency f , as described in Figure 1. (Note that this three-dimensional definition of \mathbf{u} is not equal to the two-dimensional version used in spherical harmonic CMB derivations.)

The contributions to the neutral hydrogen emission $\Delta I_T(\mathbf{u})$ can be separated into a spin temperature component $C(\mathbf{u})$ and a density and ionization fraction term $\rho_{H_I}/\langle \rho_H \rangle$, where ρ_H and ρ_{H_I} are the density of hydrogen and neutral hydrogen, respectively, and angle brackets $\langle \rangle$ denote the average. For a baryon density $\Omega_b h^2 = 0.02$ and a helium fraction $Y = 0.24$, C is given by

$$C_K \equiv (2.9 \text{ mK}) h^{-1} \frac{(1+z)^2 (T_s - T_{\text{CMB}})}{E(z) T_s} \quad (2)$$

in $\frac{\text{brightness temperature}}{\sqrt{\Omega_M(1+z)^3 + \Omega_k(1+z)^2 + \Omega_\Lambda}}$ units, where $E(z) \equiv$

The theoretical expectation for the cross-correlation of the true sky emission is a delta function given by

$$\langle \Delta I_T(\mathbf{u}) \Delta I_T^*(\mathbf{u}') \rangle = \langle |\Delta I_T(\mathbf{u}')|^2 \rangle \delta(\mathbf{u} - \mathbf{u}') d^3 \mathbf{u}'. \quad (3)$$

However, correlations are introduced by the finite field of view and bandwidth of the experiment. The correlation between two measured $\Delta \tilde{I}(\mathbf{u})$ values (no subscript T for measured value) is then given by

$$\begin{aligned} C_{ij}^I &\equiv \langle \Delta \tilde{I}(\mathbf{u}_i) \Delta \tilde{I}^*(\mathbf{u}_j) \rangle \\ &= \int P_{H_I}(|\mathbf{u}|) W(\mathbf{u}_i - \mathbf{u}) W^*(\mathbf{u}_j - \mathbf{u}) d\mathbf{u}, \end{aligned} \quad (4)$$

where $W(\mathbf{u}_i - \mathbf{u})$ is the window function given by the field of view and bandwidth of the array and $P_{H_I}(\mathbf{u}) \equiv \langle |\Delta I_T(\mathbf{u})|^2 \rangle \delta(\mathbf{u} - \mathbf{u}')$ and is approximately spherically symmetric because of the isotropy of space. The spherical symmetry is slightly broken by the evolution of the universe and redshift space distortions. Zaldarriaga et al. (2004) note that cosmic evolution is a small effect over bandwidths of ~ 10 MHz, and a very recent paper by Barkana & Loeb (2005) explores redshift space distortions and the additional cosmological information that can be

extracted using the small line-of-sight dependence these distortions introduce. A full derivation of the observed signal properties and discussion of the spherical symmetry can be found in Morales & Hewitt (2004).

Equation (4) captures the essential characteristics of the signal. The correlation between separate measurements is entirely determined by the field of view and bandwidth of the measurement and falls rapidly as the measurements move apart in the \mathbf{u} space. As the field of view and bandwidth increase, $W(\mathbf{u}' - \mathbf{u})$ becomes more centrally condensed, reducing the correlation length between measurements and increasing the expectation value of C_{ij}^I .

2.2. Thermal Noise Properties

The fundamental observable for an interferometric array is a single visibility V (Jy). The thermal noise per visibility¹ is given by

$$V_{\text{rms}} = \frac{2k_B T_{\text{sys}}}{A_e \sqrt{df} \tau}, \quad (5)$$

where T_{sys} is the total system temperature, A_e is the effective area of one antenna (m^2), df is the bandwidth of a single frequency channel (Hz), and τ is the total integration time for that visibility measurement (s).

Moving to the Fourier representation, the total noise for every measurement $\Delta I^N(\mathbf{u})$ can be calculated by Fourier transforming the visibilities. (The superscript N indicates contributions from the noise, and the superscript I , as used in eq. [4], indicates signal contributions.) Since the noise contributions to the visibilities are Gaussian distributed with zero mean, $\Delta I^N(\mathbf{u})$ will also be Gaussian distributed with zero mean. Since the rms of $\Delta I^N(\mathbf{u})$ is constant for all \mathbf{u} , it can be easily calculated from the $\eta = 0$ term and the average visibility rms:

$$\begin{aligned} \Delta \tilde{I}_{\text{rms}}^N(u, v, 0) &= \int V_{\text{rms}}(u, v, f) df \\ &= \sum^{B/df} V_{\text{rms}}(u, v, f) df, \end{aligned} \quad (6)$$

where B is the total bandwidth of the measurement. The rms of the sum is $\sqrt{N} = (B/df)^{1/2}$ times the average rms of V times df and is given by

$$\Delta \tilde{I}_{\text{rms}}^N = \frac{2k_B T_{\text{sys}} \sqrt{B}}{A_e \sqrt{\tau}}. \quad (7)$$

¹ In eq. (5), V_{rms} is implicitly averaged over all of the polarizations observed at a given location (up to three for very wide field detectors). For most ground-based arrays there are two polarizations, and T_{sys} is reduced by $\sqrt{2}$ from that of a single dipole. Alternatively, T_{sys} can be defined as the system temperature of a single polarization, and the number of independent visibility points in eq. (12) can be increased by the number of polarizations.

It is convenient to rewrite the effective area and bandwidth in terms of the physical size of the antenna dA (m^2) and the inverse of the bandwidth range $d\eta$ (Hz^{-1}):

$$\Delta \tilde{I}_{\text{rms}}^N = \frac{2k_B T_{\text{sys}}}{\epsilon dA d\eta \sqrt{B\tau}}. \quad (8)$$

In physical terms, $dA d\eta$ represents the approximate dimensions of the volume averaged by the correlator in the Fourier space, with the efficiency ϵ representing the collecting efficiency of the array both spatially within an antenna and in frequency.

To compare with the correlation matrix of the signal C_{ij}^I , we need to determine the correlation matrix of the noise,

$$C_{ij}^N(\mathbf{u}) = \langle \Delta \tilde{I}^N(\mathbf{u}_i) \Delta \tilde{I}^{N*}(\mathbf{u}_j) \rangle \quad (9a)$$

$$= \langle |\Delta \tilde{I}^N(\mathbf{u})|^2 \rangle \delta_{ij}. \quad (9b)$$

Because the thermal noise is random, $\langle \Delta \tilde{I}^N(\mathbf{u}) \rangle$ is Gaussian distributed with zero mean and rms $\Delta \tilde{I}_{\text{rms}}^N(\mathbf{u})$ given by equation (8). The expected distribution of $\langle |\Delta \tilde{I}^N(\mathbf{u})|^2 \rangle$ is Rayleigh distributed and $\langle |\Delta \tilde{I}^N(\mathbf{u})|^2 \rangle$ is exponentially distributed with rms $2[\Delta \tilde{I}_{\text{rms}}^N(\mathbf{u})]^2$. This gives the rms of the noise correlation matrix,

$$[C_{ij}^N(\mathbf{u})]_{\text{rms}} = 2 \left(\frac{2k_B T_{\text{sys}}}{\epsilon dA d\eta} \right)^2 \frac{1}{B\tau} \delta_{ij}. \quad (10)$$

Because of sky rotation, the values of \mathbf{u} observed by any given pair of antennas are a function of time. Instead of using i and j to label the observed baselines, equivalently the Fourier space can be divided into a large number of cells with i and j labeling the cells (this also applies to eqs. [4] and [9]). The noise in an analysis cell is then given by

$$[C_{ij}^N(\mathbf{u})]_{\text{rms}} = 2 \left(\frac{2k_B T_{\text{sys}}}{\epsilon dA d\eta} \right)^2 \frac{1}{B\bar{n}(\mathbf{u})t} \delta_{ij}, \quad (11)$$

where $\bar{n}(\mathbf{u})$ is the time average number of baselines in an observing cell and t is the total observation duration. For many realistic arrays $\bar{n}(\mathbf{u})$ may range from >1 at short distances because of redundant baselines to $\ll 1$ on longer baselines. The effects of array configuration on the power spectrum sensitivity are explored in § 4.

In principle, equations (4), (9b), and (11) contain all the information required to calculate the sensitivity of any given array and observing program. Using a simulation of the detector array and observing strategy, the observed Fourier space can be divided into many small cells, with the signal strength and correlation for the cells given by equation (4) and the uncertainty in each cell due to thermal noise given by equation (11).² This allows the layout of the array and the observing strategy to be accurately included in the sensitivity calculation.

Equation (11) can be further simplified by making use of the approximate spherical symmetry of the signal to average over all of the cells within a spherical annulus. Except at the shortest baselines, typical arrays have a large number of independent

cells in each annulus, and in this limit the mean of the $C_{ij}^N(\mathbf{u})$ measurements will become Gaussian distributed with rms:

$$[C_{ij}^N(\mathbf{u})]_{\text{rms}} \approx 2 \sqrt{\frac{d^3 u'}{2\pi |\mathbf{u}|^2 du}} \left(\frac{2k_B T_{\text{sys}}}{\epsilon dA d\eta} \right)^2 \frac{1}{B\bar{n}(\mathbf{u})t}. \quad (12)$$

The

$$\sqrt{\frac{d^3 u'}{2\pi |\mathbf{u}|^2 du}}$$

term is simply $N^{-1/2}$, where N is the number of cells within an annulus, with $d^3 u'$ as the size of the Fourier cells, du the width of the annulus, and the 2π term being due to the Hermitian nature of the visibility measurements limiting the summation to a half-sphere.

Equation (12) can be used to directly calculate a close approximation of the sensitivity as a function of wave number (one-dimensional). While equations (4), (9b), (11), and (12) allow calculation of the power spectrum sensitivity, the implications for array design are not immediately obvious. In §§ 3 and 4 we explore the scaling behavior of these equations and the implications for array design.

3. SCALING RELATIONSHIPS

Looking closely at equation (4) for the signal properties reveals two important characteristics. First, the correlation length is inversely proportional to the field of view and bandwidth of the observation. For many interferometric arrays at low radio frequencies, the incident electric field is directly sampled by simple dipole or similar detector elements. Because digitization and correlation is still relatively expensive compared to the cost of a single detection element, it is common to use a beamformer to combine the data from a small group of elements into one ‘‘antenna.’’ The field of view of an observatory is roughly equal to the inverse of the physical extent of the beam-formed antennas, and we identify dA in our derivation as the area of one beam-formed region. Thus, as the size of the antennas shrinks, the field of view expands, allowing a larger portion of the sky to be simultaneously observed and reducing the correlation length of the power spectrum.

We can use this to go a step farther and choose $dA d\eta$ as the cell size for the analysis. All measurements that fall within one cell will then be highly correlated and measurements in all other cells will be largely independent. We can then make the approximation that

$$C_{ij}^I(\mathbf{u}) \approx \langle |\Delta \tilde{I}(\mathbf{u})|^2 \rangle \delta_{ij} = \int P_{\text{H}1}(\mathbf{u}) |W(\mathbf{u}' - \mathbf{u})|^2 d^3 \mathbf{u}'. \quad (13)$$

Since the window function $W(\mathbf{u}' - \mathbf{u})$ is sharply peaked, the magnitude of the signal C_{ij}^I is proportional to the integral of $|W(\mathbf{u}' - \mathbf{u})|^2$. By Parseval's relation this gives

$$C_{ij}^I \propto \frac{\epsilon^2}{dA d\eta}. \quad (14)$$

Rewriting equation (12) with the cell size $dA d\eta$ gives us the uncertainty due to thermal noise in our measurement of the EOR power spectrum within an annular shell of width du :

$$[C_{ij}^N(\mathbf{u})]_{\text{rms}} \approx 2 \sqrt{\frac{dA d\eta}{2\pi |\mathbf{u}|^2 du}} \left(\frac{2k_B T_{\text{sys}}}{\epsilon dA d\eta} \right)^2 \frac{1}{B\bar{n}(\mathbf{u})t}, \quad (15)$$

² Note that the distribution of $C_{ij}^N(\mathbf{u})$ for each cell is exponentially distributed, not Gaussian.

TABLE 1
SCALING RELATIONSHIPS

Equation (No.)	$A_t _{dA}$	$A_t _{N_t}$	$dA _{A_t}$	B	$ \mathbf{u} $	t
C_{ij}^I (14).....	...	A_t^{-1}	$(dA)^{-1}$	B
ΔI_{rms}^N (18).....	...	A_t^{-1}	...	$B^{1/2}$...	$t^{-1/2}$
$\left[C_{ij}^N(\mathbf{u}) \right]_{\text{rms}}$ (15).....	A_t^{-2}	$A_t^{-5/2}$	$(dA)^{-1/2}$	$B^{1/2}$	$[\mathbf{u} \bar{n}(\mathbf{u})]^{-1}$	t^{-1}
Power Spectrum S/N.....	A_t^2	$A_t^{3/2}$	$(dA)^{-1/2} \propto \text{FOV}$	$B^{1/2}$	$ \mathbf{u} \bar{n}(\mathbf{u})$	t

NOTE.—This table lists the scaling relationships of the key equations. In order, the variables in each column are: total array area holding the size of each antenna constant $A_t|_{dA}$ (adding antennas), total array area holding the number of antennas and distribution constant $A_t|_{N_t}$ (increasing antenna size), the size of each antenna with the total array area held constant $dA|_{A_t}$ (dividing area into more small antennas), the total bandwidth B , the sensitivity as a function of wavenumber length $|\mathbf{u}|$, and the total observing time t .

where the size du of the annular bins can be arbitrarily chosen to best constrain the theory. In the limit that the noise uncertainty dominates the “cosmic variance” uncertainty introduced by the finite number of measurements ($S/N \ll 1$ for each cell), we can divide the expected signal by the rms in an spherical annulus to determine the approximate signal-to-noise ratio for the EOR power spectrum. We can then vary equations (14) and (15) with respect to different parameters to get the scaling relationships shown in Table 1. As the thermal noise becomes small these scaling laws must be modified, but Table 1 can help guide experimentalists on how design choices affect the sensitivity of an array to the EOR power spectrum.

From a statistical standpoint the natural quantity to measure is the power spectrum, which is defined as the square of the intensity. This leads to surprising effects, such as the uncertainty of the power spectrum being inversely proportional to the integration time t instead of \sqrt{t} . It should be noted that this effect is not really physical and the constraints on the underlying parameters (Ω_b , T_{sys} , etc.) are independent of the basis chosen. However, not all scaling relations are squared. Certain parameters, such as the bandwidth, do not decrease the uncertainty of an individual power measurement but instead add independent power measurements, and the sensitivity scales with the square root of the number of measurements. To help work through all of the various combinations in the table, the following list explains the behavior observed in each column of the table.

Adding antennas ($A_t|_{dA}$).—Adding collecting area by adding more antennas of the same size (dA held constant) increases the sensitivity of the power spectrum measurement as A_t^2 . This dependence comes entirely through the average number of measurements per cell $\bar{n}(|\mathbf{u}|)$. Because the size of the antennas is constant, the cell size remains the same while the number of visibilities increases as the square of the number of antennas, increasing $\bar{n}(|\mathbf{u}|) \propto A_t^2$. Of course, the correlation load also increases proportional to A_t^2 , which can be a significant expense.

Increasing antenna size ($A_t|_{N_t}$).—Another alternative for adding collecting area is to increase the size of each antenna while leaving the number and distribution of antennas the same. The advantage of this scheme is that the correlation load is unchanged; however, the gain in sensitivity is only proportional to $A_t^{3/2}$, because the field of view of the array is reduced, effectively decreasing the number of independent measurements. Mathematically, this can be seen by scaling with respect to dA , with $\bar{n}(|\mathbf{u}|) \propto dA$, since the average number of measurements per cell increases with the cell size.

Fewer elements per antenna ($dA|_{A_t}$).—An alternative to adding collecting area is to simply increase the number of antennas by putting fewer detection elements into each antenna group.

This increases the correlation load, but the sensitivity also increases with $dA^{-1/2}$, because the field of view increases. Mathematically, vary the equations with respect to dA again, but this time $\bar{n}(|\mathbf{u}|) \propto dA^{-1}$, because the total number of visibility measurements scales as dA^{-2} but the average increases linearly with the cell size.

Increasing bandwidth (B).—Increasing the bandwidth adds entirely new measurements without increasing the sensitivity of the array to the line emission of individual H I regions, so the sensitivity scales with the number of new measurements as $B^{1/2}$. Mathematically, $d\eta \propto B^{-1}$ and the density of measurements per cell $\bar{n}(|\mathbf{u}|)$ is independent of the bandwidth (cell size decreases with increase in number of frequency channels). The total bandwidth that can be used in one power spectrum measurement is limited to of order 10 MHz by cosmic evolution. However, additional bandwidth can be used to make independent power spectrum measurements during different epochs to constrain the evolution of the power spectrum.

Sensitivity as a function of wavenumber ($|\mathbf{u}|$).—As one moves to larger wavenumbers (smaller length scales), the number of cells increases as $|\mathbf{u}|^2$, leading to a linear dependence of the sensitivity on $|\mathbf{u}|$. Of course, this is very sensitive to the density of measurements at that wavenumber $\bar{n}(|\mathbf{u}|)$, as discussed in § 4.

Increasing integration time (t).—Increasing the total observation time decreases the uncertainty on each measurement, leading to a linear increase in sensitivity with duration. This somewhat counterintuitive result is because the power spectrum is related to the square of the intensity.

It should be remembered that these scaling relationships are only valid when the signal-to-noise ratio is small in each cell. Halverson (2002, chap. 6, § 5) gives a nice description of the transition from noise- to statistics-dominated uncertainty and the scaling within the noise-dominated regime for CMB interferometers. These scaling relationships can help array designers determine the effects of their design choices and are useful for comparing the sensitivity of different EOR arrays. In § 4 the effects of antenna placement are further explored.

4. EFFECTS OF ARRAY CONFIGURATION

One of the unusual properties of interferometric arrays is that the distribution of visibility measurements is easily adjusted by altering the layout of the antennas. This freedom allows one to fine-tune the characteristics of the array to maximize the scientific return. In this section we explore the effects of antenna layout on the EOR power spectrum sensitivity.

The quantity $\bar{n}(|\mathbf{u}|)$ represents the average number of measurements per Fourier cell in a spherical annulus of radius $|\mathbf{u}|$. This can be calculated from the average number of measurements

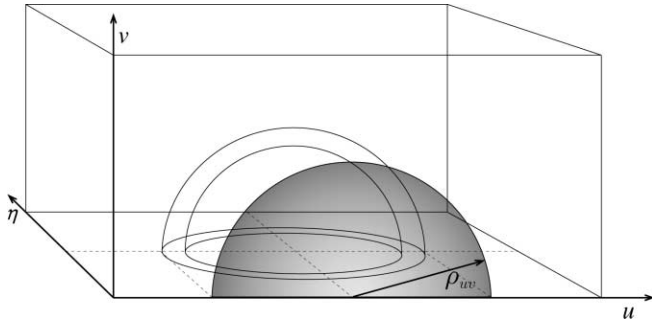


FIG. 2.—Measurement of the power spectrum at a scale $|\mathbf{u}|$ is performed by combining all of the measurements within a spherical annulus at that diameter, as shown in this figure (the origin is at the center of the annulus where the dashed lines cross). The shaded region shows the contribution of antenna baselines in the u - v plane to this measurement, with dark indicating a higher contribution. All baselines $\rho_{uv} \leq |\mathbf{u}|$ contribute to the measurement with a limb brightening functional distribution. Even very short baselines contribute information at high $|\mathbf{u}|$ because of the spatial information encoded in the frequency dimension. The presence of the third dimension changes the characteristics of the measurement and makes EOR experiments less sensitive to the antenna distribution than similar CMB interferometers.

in each individual cell $\bar{n}(\mathbf{u})$ by averaging over all the cells at that annulus:

$$\bar{n}(\mathbf{u}) = \frac{\int_0^\pi \int_0^\pi \bar{n}(\mathbf{u}) |\mathbf{u}|^2 \sin \theta \, d\phi \, d\theta}{\int_0^\pi \int_0^\pi |\mathbf{u}|^2 \sin \theta \, d\phi \, d\theta}, \quad (16)$$

where θ is measured from the η axis, and ϕ is the azimuthal angle and ranges from $0 \rightarrow \pi$, since we only integrate over half the sphere because the visibilities are Hermitian.

This relationship can be simplified by concentrating on the spatial distribution of the visibility measurements. If we neglect the small distortion introduced by fractional bandwidth, the density of measurements per cell is constant for all cells at a position u, v , independent of η . This is because each baseline measures all frequency values, thus the density of measurements is just a function of u and v . If we use polar coordinates ρ_{uv} and ϕ to represent the position of a baseline in the u, v plane (see Fig. 2), equation (16) can be simplified to

$$\bar{n}(\mathbf{u}) \approx \frac{1}{\pi |\mathbf{u}|} \int_0^\pi \int_0^\pi \bar{n}(\phi, \rho_{uv}) \frac{\rho_{uv}}{\sqrt{|\mathbf{u}|^2 - \rho_{uv}^2}} \, d\phi \, d\rho_{uv} \quad (17)$$

after carrying out the integral in the denominator and changing variables. The $\bar{n}(\phi, \rho_{uv})$ term is simply the average number of baselines within a two-dimensional cell in the u - v plane during the course of the observation. For many experiments the u - v coverage is very nearly azimuthally symmetric, allowing one to simplify even further to obtain

$$\bar{n}(\mathbf{u}) \approx \frac{1}{|\mathbf{u}|} \int_0^{|\mathbf{u}|} \bar{n}(\rho_{uv}) \frac{\rho_{uv}}{\sqrt{|\mathbf{u}|^2 - \rho_{uv}^2}} \, d\rho_{uv}. \quad (18)$$

Under closer inspection, equation (18) provides a very interesting result: the sensitivity of the array at a given scale $|\mathbf{u}|$ depends on all the visibility measurements with a spacing equal to or less than this scale. The very shortest baselines still contribute to measurements normally associated with much larger antenna spacings. The reason for this effect is the three-dimensional distribution of the measurements as shown in Figure 2. Because spatial information related to the line-of-sight distance is

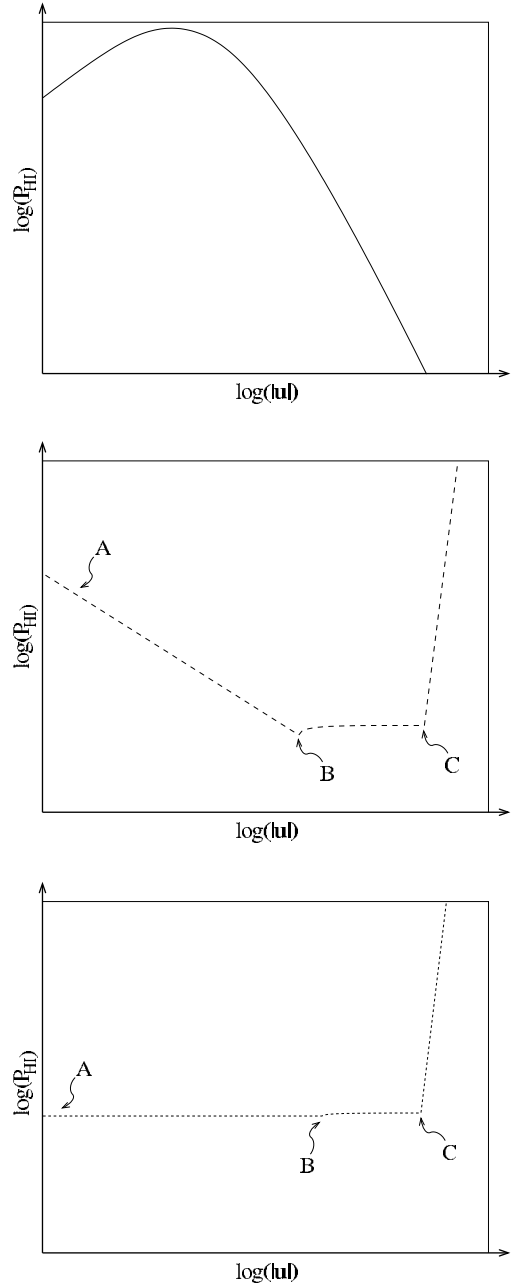


FIG. 3.—This series of cartoons shows the shape of the power spectrum, showing the edge effects and the sensitivity as a function of $|\mathbf{u}|$ for different antenna distributions. Since the scale depends strongly on the features of a particular array, it has been omitted to focus on the general characteristics. The top panel shows the power spectrum signal for a hot, fully neutral medium. The middle and bottom panels show the uncertainty due to thermal noise (noise power spectrum, for sensitivity in bins of constant logarithmic size multiply by $|\mathbf{u}|^{-1}$). The middle panel has the distribution for a uniformly sampled u - v plane, and the bottom panel has a ρ_{uv}^{-1} distribution similar to that found in centrally condensed distributions. Point B indicates the largest baseline of the array, and point C the length scale associated with the frequency channel width. Typically, C is at a larger $|\mathbf{u}|$ than B, and the sensitivity of the array extends to length scales normally associated with larger baselines. This ability to measure short spatial scales with the frequency information on short baselines favors the building of compact arrays. At the small baselines indicated by point A, the limited number of measurements becomes important, increasing the uncertainty above that indicated by the thermal noise curve (similar to “cosmic variance” effects). In addition, for centrally condensed arrays, the ρ_{uv}^{-1} visibility distribution can only be maintained until neighboring antennas touch, leading to additional increases at short baselines.

encoded in the observed frequency, very short baselines still contain information about very large $|\mathbf{u}|$ at the appropriate η value. The weighting of the baseline contributions has the same pattern as limb brightening. This means that the sensitivity of an EOR interferometer as a function of scale is fundamentally different than a CMB interferometer. Some of the sensitivity distributions that have appeared in the literature implicitly assume a single frequency of observation (two-dimensional) and do not accurately represent the scale dependence of proposed measurements.

Figure 3 shows the scale dependence of the sensitivity for two example antenna distributions. The uniform u - v coverage distribution is very difficult to realize in practice, but it does approximate the u - v distribution generated by a ring of antennas and has been used as a simplifying assumption in the literature. The other distribution is for a centrally condensed array with a $\bar{n}(\rho_{uv}) \propto \rho_{uv}^{-1}$ distribution, approximately the distribution given by a centrally condensed antenna distribution. The highest spatial frequency that can be observed in the η dimension is set by the inverse of the frequency channel resolution and is determined by the design of the correlator. For most interferometers, narrow channel widths lead to the η dimension of the observation extending to much larger values than the u and v dimensions. This leads to edge effects where the annulus becomes larger than the longest baseline and then larger than the η extent (see Fig. 3).

The ideal antenna configuration depends both on the scales of $|\mathbf{u}|$ that provide the best differentiation between models and the need to minimize systematics. Neglecting systematics favors very compact arrays, since short baselines will still contribute to large $|\mathbf{u}|$ measurements through the frequency domain. However, realistic EOR interferometers are all expected to include longer baselines. These longer baselines are crucial for identifying and removing a host of systematic effects, such as the point-source foreground, ionospheric refraction, radio interfer-

ence, and radio transients. Determining the optimum array layout will require an accurate model of the expected signal, the contaminating effects, and the analysis method, but it will likely result in a centrally condensed array with a diameter of a couple of kilometers.

5. CONCLUSION

This paper has developed the formalism needed to calculate the power spectrum sensitivity of multiwavelength epoch of reionization (EOR) observations and has explored the implications for array design. By examining the scaling relationships and the effects of antenna distribution on the sensitivity, design trade-offs can be balanced against one another. It is hoped that this work will help optimize the design of low-frequency radio telescopes for EOR observations.

In future work we will use the results from § 2.2 to develop a full simulation of the three-dimensional Fourier EOR analysis. This will allow us to accurately determine the sensitivity of specific arrays, including the effects of antenna distribution and observing strategy. The analysis framework will also allow us to explore the effects of cosmic variance, foreground contamination, ionospheric calibration errors, and instrumental polarization errors and will build the basis of an analysis package for future EOR observatories.

I would like to thank Colin Lonsdale, Roger Cappallo, and Jackie Hewitt for carefully reading and correcting early drafts. I would also like to thank the entire Mileura Wide-field Array team for blazing the path toward building a premier EOR observatory in Western Australia. This work has been supported by NSF grant AST0121164.

REFERENCES

- Barkana, R., & Loeb, A. 2005, Phys. Rev. Lett., submitted (astro-ph/0409572)
 Bharadwaj, S., & Ali, S. K. S. 2004, MNRAS, 352, 142
 Di Matteo, T., Perna, R., Abel, T., & Rees, M. J. 2002, ApJ, 564, 576
 Furlanetto, S., Zaldarriaga, M., & Hernquist, L. 2004a, ApJ, 613, 1
 Furlanetto, S., Zaldarriaga, M., & Hernquist, L. 2004b, ApJ, 613, 16
 Halverson, N. W. 2002, Ph.D. thesis, California Institute of Technology
 Morales, M. F., & Hewitt, J. 2004, ApJ, 615, 7
 Zaldarriaga, M., Furlanetto, S. R., & Hernquist, L. 2004, ApJ, 608, 622